24th COBEM - 2017

24th ABCM International Congress of Mechanical Engineering
December 3-8, 2017, Curitiba, PR, Brazil

COBEM-2017-2841
THE EFFECT OF THE RADIATIVE PROPERTIES IN POROUS MEDIA COMBUSTION

Roberto C. Moro Filho
Escola de Ciencias e Tecnologia
Universidade Federal do Rio Grande do Norte
Caixa Postal 1524, Campus Universitário Lagoa Nova
59072-970 – Natal – RN - Brasil
moro@ect.ufrn.br

Abstract. *The present work examines numerically the effect of thermal radiation in porous burners under local thermal non-equilibrium condition. The radiative transfer equation (RTE) is solved by discrete ordinate method (DOM) in a two-dimensional axisymmetric cylindrical participating media. Emission and absorption by the porous media were taken into consideration and the S12 quadrature was used to solve the RTE. The equations of mass continuity, momentum and energy are written for an elementary representative volume yielding a set of equations valid for the entire computational domain. These equations are discretized using the control volume method and the resulting system of algebraic equations is relaxed with the SIMPLE method. The reactor simulated has two different porous regions with different materials and, therefore, different optical properties. A sensitivity study of the extinction coefficient on the temperatures and species are examined. The results show that the extinction coefficient has a strong influence on the position where the flame stabilizes.*

Keywords: *Combustion, porous media, thermal radiation, numerical simulation.*

1. INTRODUCTION

Combustion in porous media occurs in a wide range of processes. Household heating combustion, systems based on fluidized bed combustion, catalytic reactors, in-situ combustion for oil recovery, are a few examples of such applications.

Studies on macroscopic transport modeling of incompressible flows in porous media have been based on the volume-average methodology for either heat or mass transfer. The accuracy of continuum models relies on the effective transport properties adopted in the calculations. The determination of the effective transport parameters suffers from several drawbacks. The analysis of transport phenomena in reticulate porous ceramic (RPC) is complex, some of the pores are open, some are closed and some are partly open and partly closed. Even samples of the same manufacturer show differences in the mean pore diameter. The geometry, shape and size distribution of the pores varies with the method of manufacturing. The author of the present article has been investigating the effective properties of RPCs through the numerical simulations of radiant porous burners. The sensitivity analyses of the effective thermal conductivity and the Rosseland mean attenuation coefficient were presented by Moro and Pimenta (2011). The correlations to the Nusselt Number obtained by the traditional methods and the effect on the solid and fluid phase temperature distributions were presented by Moro (2013). The purpose of the present work is to investigate the effect of the optical properties on the temperature and species distributions in porous radiant burners.

2. MACROSCOPIC TRANSPORT EQUATIONS

2.1. Macroscopic continuity equation

$$\phi \frac{\partial \rho}{\partial t} + \nabla.(\rho \mathbf{u}_D) = 0 \tag{1}$$

where, $\mathbf{u}_D$ is the average surface velocity (also known as seepage, superficial, filter or Darcy velocity). Equation (1) represents the macroscopic continuity equation for an incompressible fluid.

2.2. Macroscopic momentum equation

The heuristic macroscopic momentum equation utilized in this work is found in the literature (Kaviany, 1995; Pedras, 2000) and corresponds to an attempt of the scientific community to develop an equation, based on a volume-averaged treatment of the flow field, along the lines of Navier-Stokes equation. Another desirable characteristic of this heuristic equation is that it can describe both the momentum transport through the porous media as well as that in the plain media.

$$\frac{\partial(\rho \mathbf{u}_\mathrm{D})}{\partial t} + \nabla \cdot \left(\frac{\rho \mathbf{u}_\mathrm{D} \mathbf{u}_\mathrm{D}}{\phi} \right) = -\nabla(\phi p) + \mu \nabla^2 \mathbf{u}_\mathrm{D} - \left[\frac{\mu \phi}{K} \mathbf{u}_\mathrm{D} + \frac{c_F \phi \rho |\mathbf{u}_\mathrm{D}| \mathbf{u}_\mathrm{D}}{\sqrt{K}} \right] \tag{2}$$

where the last two terms in Eq. 2, represent the Darcy-Forchheimer contribution (Pedras, 2000). The symbol K is the porous medium permeability, $c_F = 0.55$ is the form drag coefficient (Forchheimer coefficient), p is the intrinsic (volume-averaged on fluid phase) pressure of the fluid, ρ is the fluid density and is a function of temperature, μ represents the fluid dynamic viscosity and ϕ is the porosity of the porous medium.

2.3. Macroscopic Two-Energy Equations Model

In this work the effects of dispersion and tortuosity are neglected.

$$\left\{ \left(\rho c_p\right)_f \phi \right\} \frac{\partial T_f}{\partial t} + \left(\rho c_p\right)_f \nabla \cdot \left(\mathbf{u}_D T_f\right) = \nabla \cdot \left\{ \mathbf{K}_{eff,f} \cdot \nabla T_f \right\} + h_v \left(T_s - T_f\right) + \phi \sum_{k=1}^{Nsp} \dot{w}_k M_k h_k \tag{3}$$

and

$$\left\{ (1-\phi) \left(\rho c_p\right)_s \right\} \frac{\partial T_s}{\partial t} = \nabla \cdot \left\{ \mathbf{K}_{eff,s} \cdot \nabla T_s \right\} - h_v \left(T_s - T_f\right) - \nabla \cdot \mathbf{q_r} \tag{4}$$

represent the energy equation for fluid and solid phase, respectively, where, T_f and T_s are the intrinsic volume average of the temperatures of the fluid phase and solid phase (Kaviany, 1995; Saito, 2006), h_v is the volumetric heat transfer coefficient and $\mathbf{K}_{eff,f}$ and $\mathbf{K}_{eff,s}$ are the effective conductivity tensors for the fluid and the solid phase, respectively, given by:

$$\mathbf{K}_{eff,s} = \left[\phi k_f \right] \mathbf{I} \tag{5}$$

$$\mathbf{K}_{eff,s} = (1-\phi)[k_s] \mathbf{I} \tag{6}$$

where, k_f and k_s are the thermal conductivities for the fluid and for the solid, respectively.

2.4. Thermal radiation modeling

In the present study, the solid and fluid phases were treated as a single continuous homogeneous medium. The fluid was assumed to be transparent to radiation. The structure of the solid phase was considered gray. The radiation intensity for an absorbing, emitting and scattering grey medium along a path $\hat{s}$ is governed by the radiative transfer equation [4,6]:

$$\frac{dI(\vec{r},\hat{s})}{ds} = -\beta(\vec{r}) I(\vec{r},\hat{s}) + S(\vec{r},\hat{s}) \tag{7}$$

where the extinction coefficient and the source function are:

$$\beta(\vec{r}) = \kappa(\vec{r}) + \sigma_s(\vec{r}) \tag{8}$$

$$S(\vec{r},\hat{s}) = k(\vec{r})I_b(\vec{r},\hat{s}) + \frac{\sigma_s(\vec{r})}{4\pi}\int_{4\pi} I(\vec{r},\hat{s}')\,\Phi(\hat{s}',\hat{s})d\Omega' \tag{9}$$

In equations (7), (8) and (9), $\vec{r}$ is the position vector, $\hat{s}$ is the unit vector describing the radiation direction and $I(\vec{r},\hat{s})$ is the radiative intensity at a given location $\vec{r}$, in the direction $\hat{s}$.

After the radiative intensity field is calculated solving the radiative transfer equation (R.T.E.) for different directions, the divergent of the radiative heat flux ($\nabla\cdot\mathbf{q_r}$) is found by applying the equation (10) and is presumed constant in each sub-volume of the mesh. The equation (10) represents a radiative energy balance on an infinitesimal volume.

$$\nabla\cdot\mathbf{q_r} = \kappa\left(4\pi I_b - \int_{4\pi} I\,d\Omega\right) \tag{10}$$

The second term on the right side of equation (10) represents the total intensity impinging on a point from all sides and is known as the incident radiation function G [6]:

$$G = \int_{4\pi} I\,d\Omega \tag{11}$$

2.5. Macroscopic Mass Transport Equation

$$\frac{\partial(\rho\phi y_k)}{\partial t} + \nabla\cdot(\rho\mathbf{u}_D y_k) = \nabla\cdot[\rho\mathbf{D}_{eff}\cdot\nabla(\phi y_k)] + \phi\dot{w}_k M_k \tag{12}$$

where y_k is the local mass fraction for the species k. The effective dispersion tensor D_{eff} is defined as:

$$\mathbf{D}_{eff} = \mathbf{D}_{disp} + \mathbf{D}_{diff} = \mathbf{D}_{disp} + \frac{1}{\rho}\left(\frac{\mu}{Sc}\right)\mathbf{I} \tag{13}$$

where, Sc is the Schimidt number, D_{diff} is the macroscopic diffusion tensor, and D_{disp} is the mass dispersion tensor (Mesquita, 2003). The effects of dispersion are neglected in this work, therefore, the effective dispersion tensor is given by:

$$\mathbf{D}_{eff} = \frac{1}{\rho}\left(\frac{\mu}{Sc}\right)\mathbf{I} \tag{14}$$

2.6. Boundary conditions

The figure 1 presents the boundary conditions to the cylindrical porous burner, where: $\dot{q}_s$ is the heat flux at the exit, $\dot{q}_r$ the heat flux due to the radiation and $\dot{q}_w$ the heat flux at the wall of the burner. The surface of the packed bed radiates energy to the surrounding surfaces according to the equation bellow:

$$\dot{q}_r = -K_{eff}\frac{\partial T}{\partial x} = \left(\varepsilon_{eff}\sigma T^4 - \alpha_{eff}\sigma T_\infty^4\right) \tag{15}$$

where, ε_{eff} is effective emissivity, α_{eff} is the effective absorptivity of the porous bed and T_∞ is the ambient temperature. The ε_{eff} and α_{eff} are equal to simplify the solution.

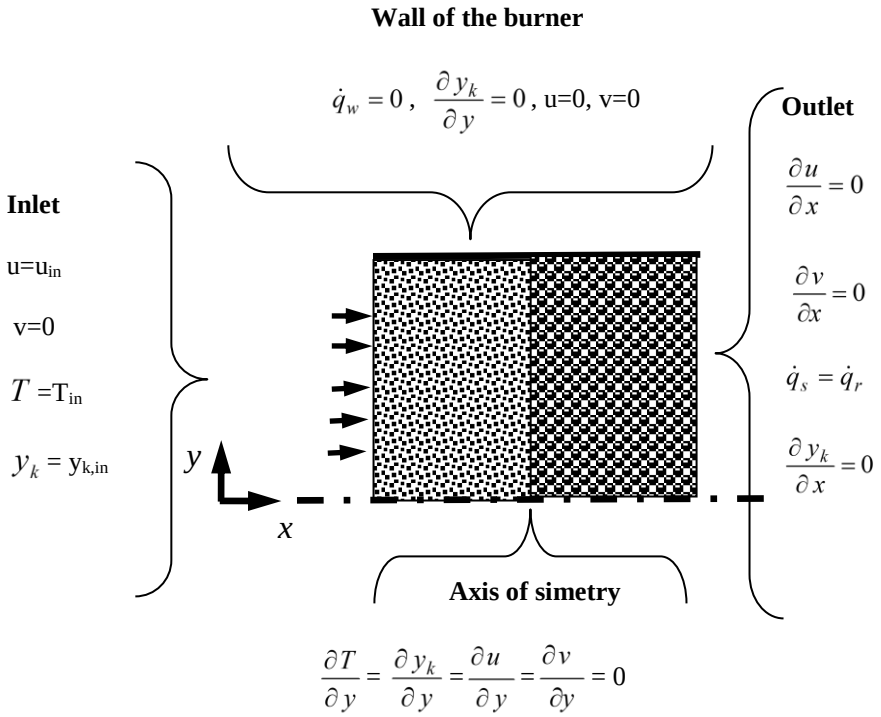

Figure 1. Boundary conditions

2.7. Combustion model

The method to solve the chemical kinetic problem utilizes two models to describe the reaction process, a global reaction mechanism is used as a first approximation, following a six step reaction mechanism.

2.7.1. One-step global mechanism

The combustion reaction is assumed to occur in a single step according to the chemical equation

$$CH_4 + 2(1+\Psi)(O_2 + 3.76N_2) \longrightarrow CO_2 + 2H_2O + 2\Psi O_2 + 7.52(1+\Psi)N_2 \quad (16)$$

where, ψ is the excess air in the reactant stream at the inlet of porous foam and is related to the equivalence ratio Φ by,

$$\Psi = \frac{1}{\Phi} - 1 \quad (17)$$

where,

$$\Phi = \frac{(y_{fu} / y_{ox})}{(y_{fu} / y_{ox})_{st}} \quad (18)$$

The ratio of fuel consumption is given by,

$$S_{fu} = \rho^2 A y_{fu} y_{Ox} \exp(-E_a / RT) \quad (19)$$

where, A is the pre-exponential factor, Ea is the activation energy and R is the universal gas constant. The gas density is updated using the ideal gas equation in the form,

$$\rho = P_0 / R^* T \quad (20)$$

where, P_0 is a reference pressure, which is kept constant during the relaxation process, and $R^* = R/M$ and M is the gas molecular mass.

2.7.2. Six-step reduced mechanism

Chang and Chen have developed a six-step reduced mechanism with an automatic computer code (CARM) from GRI-MECH 1.2:

(I) 2O = O2
(II) H + O = OH
(III) H2 + O = H + OH
(IV) O + (1/2) CH4 = (1/2) H2 + (1/2) H + (1/2) OH + (1/2) CO
(V) O + CO = CO2
(VI) O + H2O + (1/4) CO = (1/4) H2 + (1/4) H + O2 + (1/4) OH + (1/4) CH4

3. NUMERICAL MODEL

The governing equations were discretized using the finite volume procedure (Patankar, 1980) with a boundary-fitted non-orthogonal coordinate system. The system of algebraic equations was solved through the semi-implicit procedure according to Stone (1968). The SIMPLE algorithm for the pressure-velocity coupling was adopted to correct both the pressure and the velocity fields. The process starts with the solution of the two momentum equations. Then the velocity field is adjusted in order to satisfy the continuity principle. This adjustment is obtained by solving the pressure correction equation. The energy and species equations are solved using a fractional time step method (Yanenko, 1971) to eliminate the problems arising from the stiffness of the system. It was adopted the minimum residence time of the gas in all control volumes as the integration time step. Calculations start using one-step global kinetics mechanism, when the residuals reach $1x10^{-3}$ the multistep mechanism is switched on and the fractional time step method is applied (Malico *et al.*, 2000). The radiative transfer equation (RTE) is solved by discrete ordinate method (DOM) in a two-dimensional axisymmetric cylindrical participating media. Emission and absorption by the porous media were taken into consideration and the S12 quadrature was used to solve the RTE. A computational mesh of 266x34 is adopted in the simulations.

All computations were performed on an Intel(R) Xeon(R) 3.40 GHz, 32GB. For all cases, a relative convergence of 10^{-5} was specified. The grid effects on the solutions were examined by increasing the number of nodes and verifying the solutions until the results no longer changed in a specified tolerance.

4. RESULTS AND DISCUSSION

The parameters for the one-step global mechanism used as a first approximation are the same to all cases. The activation energy, Ea, and the pre-exponential factor, A, were taken from Mohamad *et al*. (1994) and are $140x10^3$ J/mol and $1x10^{10}$ $m^3kg^{-1}s^{-1}$, respectively.

4.1. Burner simulated

Figure 2 presents a two-dimensional axisymmetric geometry corresponding to the porous media burner. The reactor consists of two distinct regions with different porosities and permeabilities, the gas mixture enters at the inflow boundary on the left (preheating region), and the combustion products leave the burner at the outflow boundary on the right (combustion region). In the preheating region a mixture of 65% of zirconium oxide (ZrO_2) and 35% of alumina (Al_2O_3) was utilized, 15.74 pores per centimeter (ppcm), and 86% of porosity. In the combustion region the same material of the preheating region was utilized, with 3.9 ppcm, and 90% of porosity. The walls are impermeable and isolated with a mix of alumina (Al2O3). The numerical parameters are found in table 1.

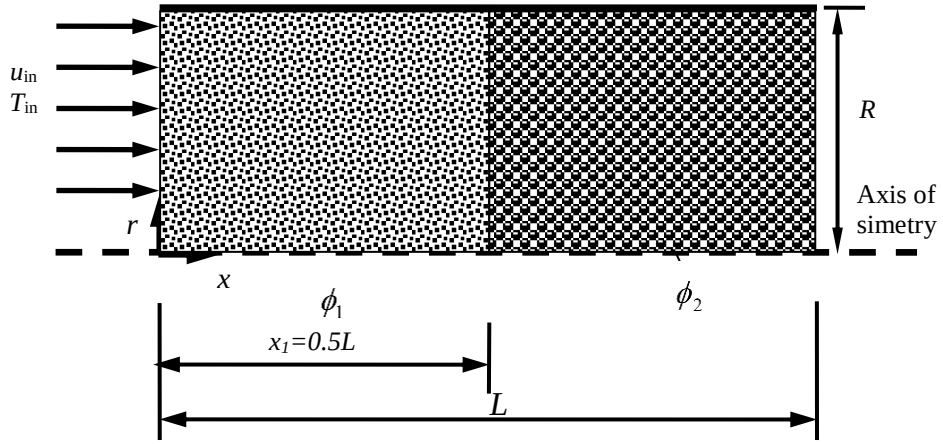

Figure 2. Geometry of a cylindrical porous burner and coordinate system

4.2. The effect of the extinction coefficient on the temperatures and flame stabilization position

In general, porous radiant burners have two porous regions, a pre-heating region and a combustion region. Different materials can be utilized in the two regions. The choice of the materials depends on the application of the porous burner, depends on the position where the flame must stabilize, the temperatures distributions, etc. The heat transport in the porous regions by radiation will depend on the optical properties of the materials utilized. The effect of the extinction coefficient on the solid phase temperature distribution is presented in Figure 3, where B1 and B2 represents the extinction coefficient of the pre-heat region and of the combustion region, respectively. The extinction coefficient is related to the attenuation of the radiation. For very high values of the extinction coefficient, the absorption is high, but the heat travels short distances before being completely attenuated. For very low values of the extinction coefficient, the energy travels long distances, but the amount of energy absorbed is low. The Figure 3 shows that for very high values and for very low values of the extinction coefficient the effect of radiation is small and the temperature profiles is close to that obtained considering a non-radiative model.

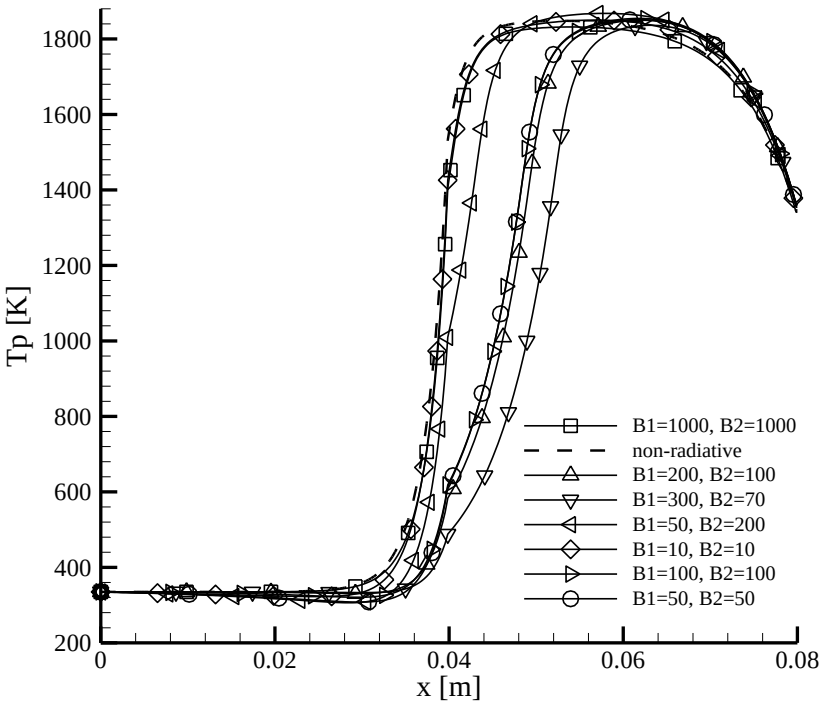

Figure 3: Solid temperatures distributions at the center line (r=0) obtained utilizing different extinction coefficients for porous matrix 1 and 2.

The Figure 4 presents the effect of the extinction coefficient on the methane mass fraction distribution. The methane is consumed very fast and its mass fraction profile can indicate the position where the flame stabilized. The Figure 4 shows that the flame position has a strong dependence on the extinction coefficient of the two porous regions. Depending on the optical properties of the material adopted in the porous burner, the flame can stabilize in the porous matrix 1 or 2.

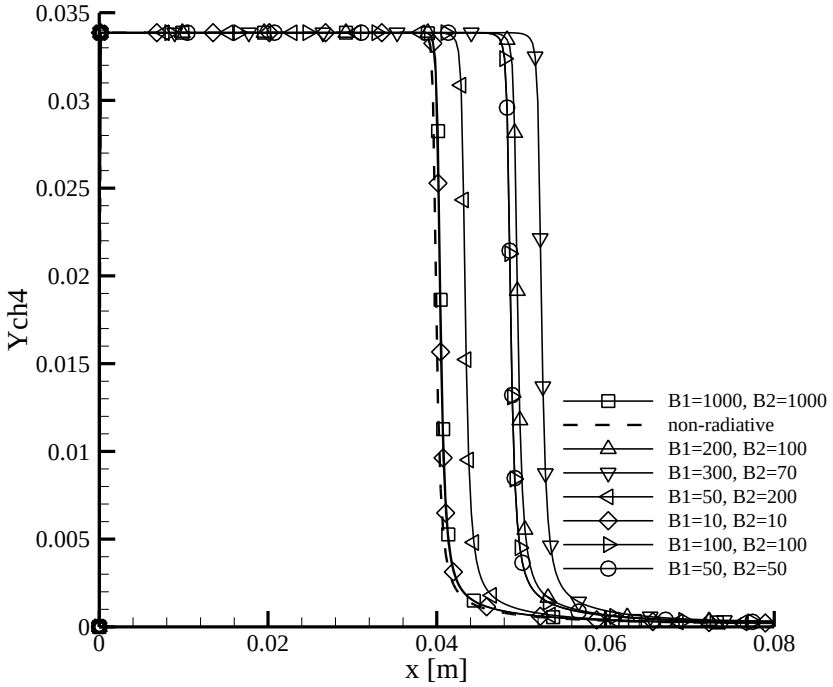

Figure 4: Methane mass fraction distributions at the center line (r=0) obtained utilizing different extinction coefficients for porous matrix 1 and 2.

The Figure 5 shows the incidence radiation profiles for different extinction coefficients. It was considered the same value of the extinction coefficient for the two porous regions. The incidence radiation is defined as the total intensity impinging on a point from all sides. For very low values of the extinction coefficient, around 10 m^{-1}, the energy travels long distances before being attenuated and the radiation, and the incidence radiation, is distributed in the two porous region. Increasing the extinction coefficient increases the amount of energy absorbed by the medium, but decreases the capacity of the energy to travel long distances before being attenuated.

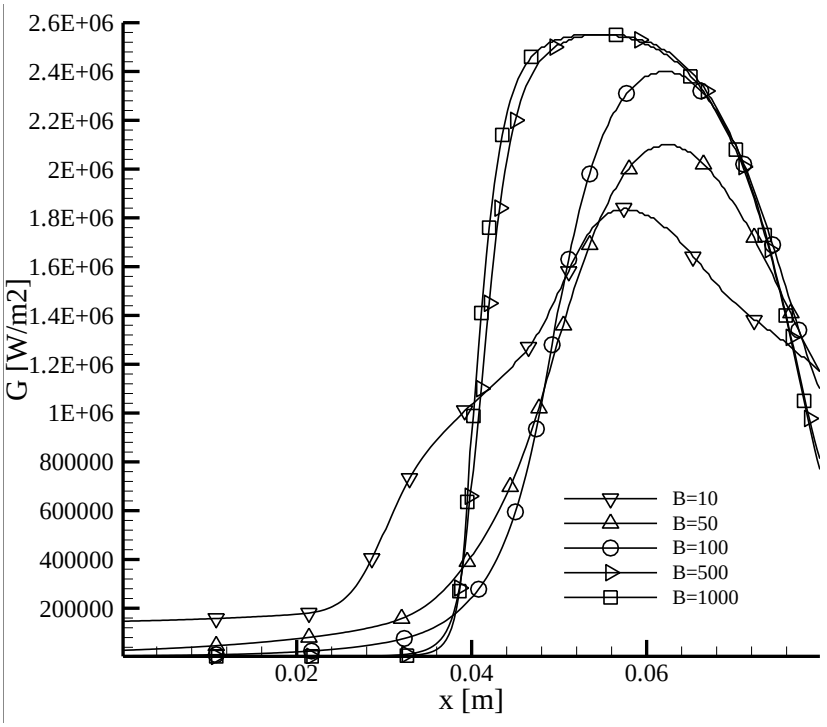

Figure 5: Incidence radiation distributions at the center line (r=0) obtained utilizing different extinction coefficients for the porous medium.

5. CONCLUSION

This study has presented the effect of the radiation heat transfer in porous burners. A sensitivity analyses was performed to determine the influence of the extinction coefficient for porous media combustion. The results show a strong dependence between the place where the flame stabilize in the porous burners and the optical properties of the materials utilized in the pre-heat region and in the combustion region. For low values of the extinction coefficient the energy can travel long distances inside the reactor before being completely attenuated, but the amount of radiative energy that travels is low. For high values of the extinction coefficient, the absorption is high, but the radiative energy travels short distances before being completely attenuated. For high values and low values of the extinction coefficient the effect of the radiation on the flame position is close to that obtained with the non-radiative model.

6. ACKNOWLEDGEMENTS

The authors are thankful to Brazilian Space Agency (AEB), for their financial support during the preparation of this work.

Table 1. Operating Conditions

Quantity	Value
Activation energy (J/mol) - Ea	$1.4x10^{8}$
Pre-exponential factor in reaction rate – A (m3/kg.s)	$1x10^{10}$
Length of the combustor – L (cm)	8
D (cm)	4
R (kJ/kmol.K)	8.3145
R* (kJ/kgK)	0.301
P_0 (kN/m2)	101.325
$y_{fuel,in}$	0.033784
T_{in} (K)	335
Matrix 1:	
K_1 (m2)	$1.477x10^{-8}$
ϕ_1	0,86
a_{v1}	1060 m^{-1}
Matrix 2:	
K_2 (m2)	$3.698x10^{-7}$
ϕ_2	0.90
a_{v2}	960 m^{-1}

7. REFERENCES

Chang, W.C., and Chen, J.Y., Reduced Mechanisms based on GRI-Mech 1.2, http://firebrand.me.berkeley.edu/griredu.html

Fu, X., Viskanta, R., Gore, J.P., 1998, Measurement and correlation of volumetric heat transfer coefficients of cellular ceramics, Experimental Thermal and Fluid Science, Vol. 17, pp. 285-293.

Kaviany. M.. 1995. Principles of Heat Transfer in Porous Media. 2nd edn. Springer. New York.

Kee, R. J., Rupley, F. M., Miller, J. A., Coltrin, M. E., Grcar, J. F., Meeks, E., Moffat, H. K., Lutz, A. E., Dixon-Lewis, G., Smooke, M. D., Warnatz, J., Evans, G. H., Larson, R. S., Mitchell, R. E., Petzold, L. R., Reynolds, W. C., Caracotsios, M., Stewart, W. E., Glarborg, P., Wang, C., Adigun, O., Houf, W. G., Chou, C. P., and Miller, S. F., Thermodynamic data is part of the CHEMKIN Collection. Chemkin Collection, Release 3.7, Reaction Design, Inc., San Diego, CA (2002).

Kuwahara, F., Shirota, M., Nakayama, A., 2000, A numerical study of the interfacial convective heat transfer coefficient in two-energy equation model for convection in porous media, International Journal of Heat and Mass Transfer, Vol. 44, pp. 1153-1159.

Malico, I., Zhou, X.Y., and Pereira, J.C.F., 2000, Two-dimensional Numerical Study of Combustion and Polutants Formation in Porous Burners, Combust. Sci. and Tech., 152, pp. 57-79.

Mesquita, M.S., 2003, Análise da dispersão mássica em meios porosos em regimes laminar e turbulento. Tese de doutorado, Instituto Tecnológico de Aeronautica, Brasil.

Mohamad, A.A., Ramadhyani, S., Viskanta, R, 1994.Modeling of Combustion and Heat-Transfer in a Pcked-Bed with Embedded Coolant Tubes, Int. J Heat and Mass Transfer. vol. 37. (8) pp.1181-1191.

Moro Filho, R. C.; Pimenta, A., 2011. A Two-Dimensional Numerical Simulation of Combustion and Heat Transfer in Radiant Porous Burners. Combustion Science and Technology. , v.183, p.370 - 389.

Moro Filho, R. C., 2013. A study of the interfacial heat transfer coefficient in porous burners, Ribeirão Preto-SP, 22th International Congress of Mechanical Engineering.

Patankar. S. V.,1980. Numerical Heat Transfer and Fluid Flow. Hemisphere. New York.

Pedras, M.H.J., 2000, Análise do Escoamento Turbulento em Meio Poroso Descontínuo. Tese de doutorado, Instituto Tecnológico de Aeronautica, Brasil.

Pereira, F.M., 2002, Medição de características térmicas e estudo do mecanismo de estabilização de chama em queimadores porosos radiantes. Tese de Mestrado, Universidade Federal de Santa Catarina, Brasil.

Petrasch, J., Meier, F., Friess, H., Steinfeld, A., 2007, Tomography based determination of permeability, Dupuit-Forchheimer coefficient, and interfacial heat transfer coefficient in reticulate porous ceramics, International Journal of

Heat and Fluid Flow, Vol. 29, pp. 315-326.
Saito, M. B., 2006, Analysis of Thermal Non-Equilibrium for Turbulent Transport in Porous Media, Tese de doutorado, Instituto Tecnológico de Aeronautica, Brasil.
Sathe, S.B., Peck, R.E., and Tong, T.W., 1990, A numeriacal analysis of heat transfer and combustion in porous radiant burners, Int. J Heat and Mass Transfer, Vol. 33, pp. 1331-1338.
Siegel, Robert, and, Howell, John, 2002, Thermal Radiation Heat Transfer, 4th edition.
Stone, H. L., 1968, Iterative Solution of Implicit Approximations of Multidimensional Partial Equations, SIAM J. Numer. Anal. vol 5, pp. 530-558.
Yanenko, N. N. (l97l). The method of fractional time steps: the solution of problems of'mathematical phisics in several variables, M . Holt (Editor), Springer-Verlag, New York.
Trimis, D., and, Durst, F., 1996, Combustion in a Porous Medium Advances and Applications, Combust. Sci. Technol, Vol. 121, pp. 153-168.

8. RESPONSIBILITY NOTICE

The author is the only responsible for the printed material included in this paper.